Three-Dimensional Finite Element Study on Stress Generation in Synchrotron X-Ray Tomography Reconstructed Nickel-Manganese-Cobalt Based Half Cell

Linmin Wu[1], Xianghui Xiao[2], Youhai Wen[3], Jing Zhang[1],*

[1]Department of Mechanical Engineering, Indiana University-Purdue University Indianapolis,

Indianapolis, IN 46202, USA

[2]X-ray Science Division, Argonne National Laboratory,

Lemont, IL 60439, USA

[3]National Energy Technology Laboratory,

Albany, OR 97321, USA

*Email: jz29@iupui.edu; Phone: 317-278-7186; Fax:317-274-9744

Abstract

In this study, the stress generation caused by phase transitions and lithium intercalation of nickel-manganese-cobalt (NMC) based half cell with realistic 3D microstructures has been studied using finite element method. The electrochemical properties and discharged curves under various C rates are studied. The potential drops significantly with the increase of C rates. During the discharge process, for particles isolated from the conductive channels, several particles with no lithium ion intercalation are observed. For particles in the electrochemical network, the lithium ion concentration increases during the discharge process. The stress generation inside NMC particles is calculated coupled with lithium diffusion and phase transitions. The results show the stresses near the concave and convex regions are the highest. The neck regions of the connected particles

can break and form several isolated particles. If the isolated particles are not connected with the electrically conductive materials such as carbon and binder, the capacity loses in battery. For isolated particles in the conductive channel, cracks are more likely to form on the surface. Moreover, stresses inside the particles increase dramatically when considering phase transitions. The phase transitions introduce an abrupt volume change and generate the strain mismatch, causing the stresses increase.

Keywords: synchrotron X-ray tomography; NMC; phase transitions; finite element; stress; diffusion

1. Introduction

Lithium ion rechargeable batteries (LIBs) are one of the most promising candidates for portable electronics and electric vehicles applications due to their high energy density [1]. Many technological improvements have been made to increase the energy density and cycle life of LIBs, including suppressing dendrites formation [2, 3], reducing side reactions [4, 5], and preventing thermal runaway [6, 7]. One of the critical challenges of LIBs is to enhance the mechanical stability of electrode materials. Diffusion induced stresses [8, 9] and phase transition [10, 11] during the operations of LIBs can cause fracture and mechanical failure. Hence, it is important to understand the stress generation in battery materials.

Many studies have been done to study the stress generation to prevent the mechanical failures of LIBs [9, 12-16]. Zhang *et al.* [14, 15] studied the diffusion induced stresses in $LiMn_2O_4$ under galvanostatic and potentiodynamic conditions using ellipsoid shaped particle model. Cheng and Verbrugge [13] investigated the strain energy of a spherically-shaped electrode particle under a periodic voltage excitation source. They evaluated the crack nucleation using strain energy density method. However, many of these studies employed single sphere particle model, and diffusion kinetics and electrochemical processes were simplified greatly. There are some attempts to simulate the stress generation of realistic microstructures in LIBs. Lim *et al.* [8] studied the diffusion induced stresses of realistic microstructures of Li_xCoO_2 and Li_xC_6 particles reconstructed by synchrotron X-Ray tomography. Wu *et al.* [17] investigated the mechanical behavior of $LiMn_2O_4$ cathode reconstructed by 2D SEM images under discharge conditions. The phase transition was not considered in the study.

Stresses caused by phase transition inside the electrode materials are detrimental to electrode particles. Phase transition can introduce abrupt volume changes to the structure, leading

3

to structure instability. However, the studies of stress generation including diffusion induced stress and phase transitions are rare. Park *et al.* [10] calculated the stresses with phase transition and intercalation in $LiMn_2O_4$ particles, but the geometry used in the model was simple shaped particles. Renganathan *et al.* [11] simulated the stress inside the porous electrode by taking advantage of the P2D model. They evaluated the stresses at the phase interface. Although the stresses caused by phase transition and Li intercalation have been considered in above works, some important features cannot be captured using homogeneous microstructures, such as the diffusion kinetics at high C rates and the geometry effect on stresses. Thus, a realistic microstructure based stress generation study with phase transition and intercalation is necessary.

In this paper, the electrochemical performance and the stress generation inside the cathode microstructure including phase transition and Li intercalation will be calculated using synchrotron X-ray reconstructed NMC half cell. The paper is organized as follows: In section 2, the details of imaging processing and reconstruction of NMC half cell are given. In section 3, a set of mathematical formulations describing the electrochemistry and the stresses in LIBs are listed. In section 4, the electrochemical performance of NMC half cell under various C rates are studied. The geometry effect on stress is discussed. The stress distributions in the particles are also analyzed. Conclusions are given in section 5.

2. Microstructure reconstruction and finite element mesh

The microstructure used for the model was obtained by synchrotron X-ray tomography at beamline 2-BM at the Advanced Photon Source, Argonne National Laboratory. The NMC cathode ($LiNi_{0.33}Mn_{0.33}Co_{0.33}O_2$) used in the experiment was from a commercial LG HE4 18650 cell. The NMC 18650 cell was disassembled in argon filled glove box, and the cathode materials were

carefully scratched off. A set of gray-scale images ware obtained with a voxel size of 0.65 μm after synchrotron X-ray tomography. The carbon and binder phase was neglected in this study, because it is hard to distinguish it from the background. It is noted that the lack of carbon and binder phase may cause isolated NMC particles. In order to reduce the computational cost, an edge preserving smoothing filter and small islands removal filters were applied followed by greyscale threshold segmentation. The resulting reconstruction was a cuboid with a dimension of 45 μm × 45 μm × 33 μm. The cross section images before and after image processing are shown in Fig. 1 (a) and (b). Overall, the images after processing preserve the major microstructural features of the unprocessed images.

In order to simulate the electrochemical performance, a three-dimensional finite element model of the NMC half cell was created. The NMC half cell was made up of cathode, electrolyte and separator domains. A separator with 10 μm thickness was added to the cathode domain (Fig. 1 (c)). The pore space in the cathode domain was filled with electrolyte. The porous structure in the separator was neglected. Two domains were meshed and imported into Comsol Multiphysics for further simulation.
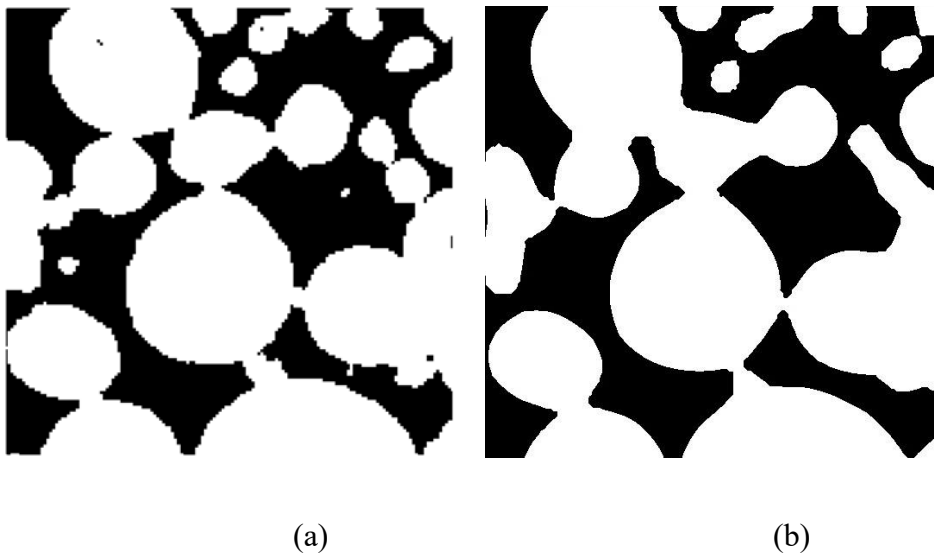
(a)   (b)
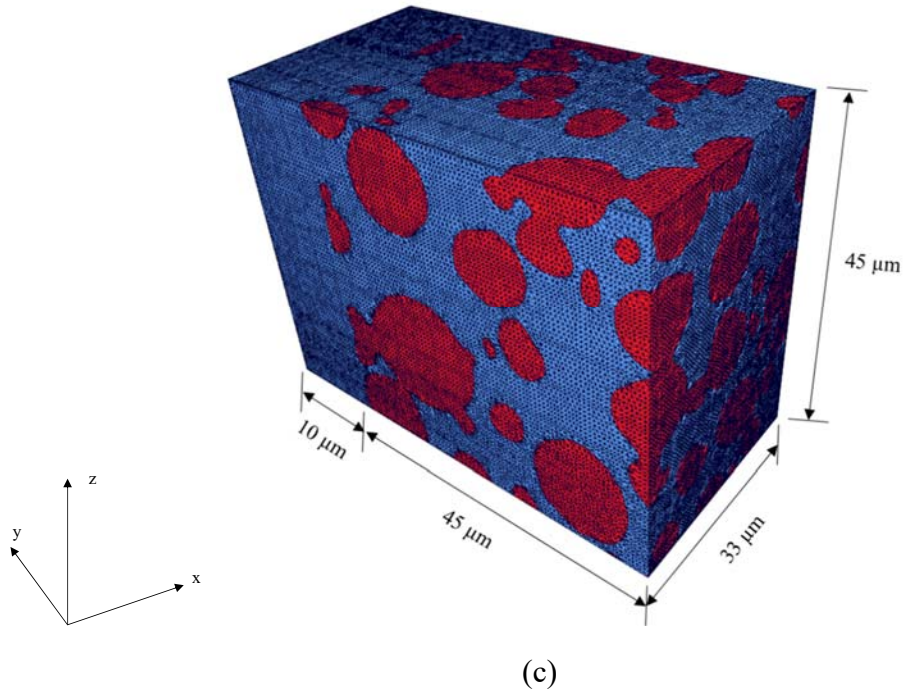
(c)

Fig. 1: (a) Raw synchrotron X-ray reconstructed NMC cathode's cross sectional view before image processing. White color represents NMC particles and black colar represents electrolyte. (b) Cross sectional view of NMC cathode after image processing. White color represents NMC particles and black colar represents electrolyte. (c) Three-dimensional finte element mesh of the NMC half cell. Red color represents NMC particles and blue color represents electrolyte.

3. Model description

The mathematical model consists of electrochemistry sub-model and mechanics sub-model. The electrochemistry model describes the species and charge transports in the NMC half cell. The mechanics model computes the mechanical stresses and diffusion induced stresses in active particles.

3.1 Electrochemistry

The electrochemistry model describing battery kinetics, mass and charge transports is based on the work of Doyle *et al.* [18] and Fuller *et al.* [19]. In order to distinguish different domains, subscript of $i = 1$ and 2 denotes the active cathode particles and the electrolyte. Here, we assume the lithium diffusivity and the electrical conductivity remain the same after the phase transition.

Active cathode particles — The charge balance in the active cathode particles follows the Ohm's law:

$$\nabla \cdot (-k_1 \nabla \phi_1) = \nabla \cdot J_1 = 0 \tag{1}$$

where k_1 is the electrical conductivity of the active cathode particles; ϕ_1 is the electrical potential and J_1 is the current density in NMC particles.

The transport of Lithium ions in active particles is described by the modified Fick's law [15, 20], which includes the effect of stresses on diffusion:

$$\frac{\partial c_1}{\partial t} + \nabla \cdot \left(-D_1 \nabla c_1 + \frac{D_1 \Omega c_1}{RT} \nabla \sigma_h \right) = 0 \tag{2}$$

where c_1 is the lithium ion concentration in solid particles; D_1 is the diffusivity of lithium ions in NMC electrode; R is the universal gas constant; T is temperature, which is set 273 K in this study; Ω is the partial molar volume of active particles; $\sigma_h = (\sigma_{11} + \sigma_{22} + \sigma_{33})/3$ is the hydrostatic stress (σ_{ij} is stress component in the stress tensor).

Electrolyte — The charge transport equation of the electrolyte phase couples the concentration of lithium ions and the electrical potential, and has the following form:

$$\nabla \cdot \left(-k_2 \nabla \phi_2 + \frac{2 k_2 RT}{F c_2} (1 + \frac{\partial \ln f_2}{\partial \ln c_2})(1 - t_+) \nabla c_2 \right) = \nabla \cdot J_2 = 0 \tag{3}$$

7

where k_2 is the electrical conductivity of the electrolyte, ϕ_2 is the electrical potential; F is the Faraday constant; c_2 is the lithium ion concentration in the electrolyte; t_+ is the transference number of positive ions, which is set 0.363 in this study; f_2 is the mean molar activity coefficient of the electrolyte.

The mass transport of lithium ions in the electrolyte is expressed as:

$$\frac{\partial c_2}{\partial t} + \nabla \cdot [-D_2 \left(1 - \frac{dlnc_0}{dlnc_2}\right) \nabla c_2 + \frac{J_2 t_+}{F}] = 0 \tag{4}$$

where D_2 is the reference lithium ion diffusivity in the electrolyte; $dlnc_0/dlnc_2$ is the concentrated solution correction to salt diffusivity; J_2 is the current density in the electrolyte. Assume the solvent concentration is not a function of the electrolyte [21], the term $dlnc_0/dlnc_2$ will be neglected. Since t_+ is a constant in this study, $\nabla \cdot (J_2 t_+/F)$ becomes zero.

Interface conditions — The chemical kinetics at the particle-electrolyte interface is described by the Butler-Volmer relationship:

$$N = \frac{i_n}{F} = \frac{i_0}{F} \times \left\{\exp\left[\frac{(1-\alpha)F\eta}{RT}\right] - \exp\left[\frac{-\alpha F\eta}{RT}\right]\right\} \tag{5}$$

where N is the flux of lithium ions; i_0 is the exchange current density; α is the cathodic charge transfer coefficient, which is 0.5 in this study; η is the overpotential at the particle-electrolyte interface.

The exchanged current density is defined as follows:

$$i_0 = Fk_0(c_2)^{1-\alpha}(c_\theta)^{1-\alpha}\left(c_{1,surf}\right)^\alpha \tag{6}$$

where k_0 is the reaction rate; $c_{1,surf}$ is the concentration of lithium ions on the surface of solid electrode; c_θ is the concentration of available vacant sites on the surface of solid particles.

The overpotential is given by:

$$\eta = \phi_1 - \phi_2 - U \tag{7}$$

where U is the open circuit potential at the interface.

3.2 Mechanics

In mechanics model, only NMC particles are simulated. The Young's modulus of liquid electrolyte is much lower than NMC particles. Hence, liquid electrolyte has little influence on the mechanical response of NMC particles. The mechanics model computes the stresses and particle deformations in active material particles. The total strain ε_{ij} contains the mechanical strain ε_{ij}^{me}, the diffusion induced strain ε_{ij}^{dis} and the phase change induced strain ε_{ij}^{ph}. The diffusion induced strain is formulated by the thermal analogy [11, 13]. The constitutive equation describing the stress and strain before phase transition is given by:

$$\varepsilon_{ij} = \varepsilon_{ij}^{me} + \varepsilon_{ij}^{dis} = \frac{1}{E}\left[(1+v)\sigma_{ij} - v\sigma_{kk}\delta_{ij}\right] + \frac{\hat{c}\Omega}{3}\delta_{ij} \tag{8}$$

where E is Young's modulus; v is Poisson's ratio; σ_{ij} is stress tensor; $\hat{c}$ is the concentration difference of lithium ions from the original value; Ω is the partial molar volume.

After phase transition, an additional strain was introduced:

$$\varepsilon_{ij} = \varepsilon_{ij}^{me} + \varepsilon_{ij}^{dis} + \varepsilon_{ij}^{ph} = \frac{1}{E}\left[(1+v)\sigma_{ij} - v\sigma_{kk}\delta_{ij}\right] + \frac{\hat{c}\Omega}{3}\delta_{ij} + \frac{W_{ph}}{3}\delta_{ij} \tag{9}$$

where W_{ph} is the volume change due to the phase transition.

The stress components obey mechanical equilibrium:

$$\sigma_{ij,j} = 0 \tag{10}$$

9

3.3 Boundary conditions and material properties

For electrochemistry model, at the right side outer boundary of the NMC electrode, a constant current density was applied. Different C rates were employed to simulate the discharge of NMC half cell. At the left hand side of the electrolyte, the electric potential is set 0 V. For all other outer surfaces, the periodic boundary conditions are applied. For mechanics model, fixed boundary conditions were applied on the outer surfaces of NMC particles.

The state of charge (SOC) is defined as the ratio of the maximum local lithium ion concentration to the stoichiometric lithium ion concentration in NMC particles ($LiNi_{0.33}Mn_{0.33}Co_{0.33}O_2$). It is reported that the $Li_xNi_{0.33}Mn_{0.33}Co_{0.33}O_2$ has a layered structrure when $0<x<1$, while it has a spinel structure when $1<x<1.2$ [22, 23]. In order to avoid the numerical diffuculty of the sudden phase transition, a linear transition zone with a width 0.05 at $x=1$ is applied. Hence, when $0<SOC<0.975$, the cathode has no phase transitions. $0.975<SOC<1.025$ is the transition zone, and $SOC>1.025$ is the region where phase transtion occur. The material properties used in the model are listed in Table 1. For electrical conductivity, lithium ion diffusivity, and $\partial(\ln f_2)/\partial(\ln c_2)$ in the electrolyte were chosen at 25 °C as provided in Ref. [24]. The open circuit potential of NMC was chosen from Ref. [25]. The reaction rate constant k_0 is 6.5×10^{-9} $m^{5/2}s^{-1}mol^{-1/2}$ [26].

Table 1: Material properties used in the model

	NMC	electrolyte
Initial concentration (mol m^{-3})	0	1000
Stoichiometric concentration (mol m^{-3})	29000	/
Electrical conductivity (S m^{-1})	10 [27]	Ref. [24]
Diffusivity (m^2 s^{-1})	7.6×10^{-13} [27]	Ref. [24]
Young's modulus (GPa)	80 [28]	/
Poisson's ratio	0.3 [28]	/
Partial molar volume (m^3 mol^{-1})	2.1×10^{-6} [29]	/
Volume change of the phase transition	0.034 [22]	/

4. Results and discussion

The mathematical model described in section 3 was implemented in Comsol Multiphysics PDE module. The simulation time step was set to 0.001 s. The NMC half cell discharged under various C rates was simulated. In this study, the NMC half cell was discharged during SOC from 0 to 1.1.

4.1 Electrochemical response

The discharge curves of the NMC half cell under 0.5 C, 1 C and 2 C are shown in Fig. 2 (a). The normalized capacity is defined as the ratio of the actual capacity and the theoretical capacity. The NMC half cell discharged at 0.5 C rate has the best voltage response. With the increase of the C rate, the voltage drops. With the same capacity, the voltage of the NMC half cell

discharged at 2 C rate is about 0.15 V lower than the cell discharged at 0.5 C. Near the normalized capacity equals to 1, the voltage difference between the half cell discharged at 0.5 C and 2 C is huge.

In order to explain the voltage reduction during the discharge, the actual polarization was calculated. In this study, the actual polarization was considered mainly due to activation polarization and concentration polarization. The average polarization of activation overpotential occurring at the electrode-electrolyte interface and concentration polarization occurring in electrolyte or NMC particles [30] is expressed as,

$$\eta_{activation} = \frac{1}{A \cdot J_{total}} \iint i_n \cdot \eta \, ds \tag{11}$$

$$\eta_{concentration} = \frac{1}{A \cdot J_{total}} \iiint J_{m,n} \cdot \frac{\partial \phi}{\partial n} \, dV \tag{12}$$

where J_{total} is applied current density; A is the cross section area of the applied current density; m =1,2 where 1 represents NMC particles and 2 represents electrolyte; n=1,2,3 is the Cartesian coordinate component; s is the area of the electrode-electrolyte interface; V is the volume of electrode or electrolyte. As shown in Fig. 2 (b), (c) and (d), the average activation overpotential is the major contribution to the total polarization. The activation overpotential is about 4 to 5 times larger than the concentration polarization. With the increase of SOC, the total polarization increases monotonically. In addition, the polarization goes up with the increasing C rates, which taking accounts into the voltage reduction phenomenon shown in Fig. 2 (a).
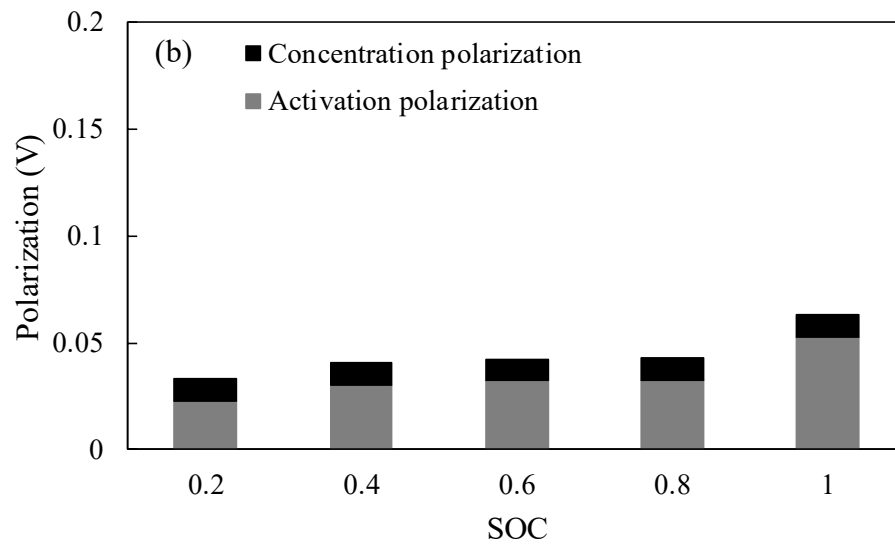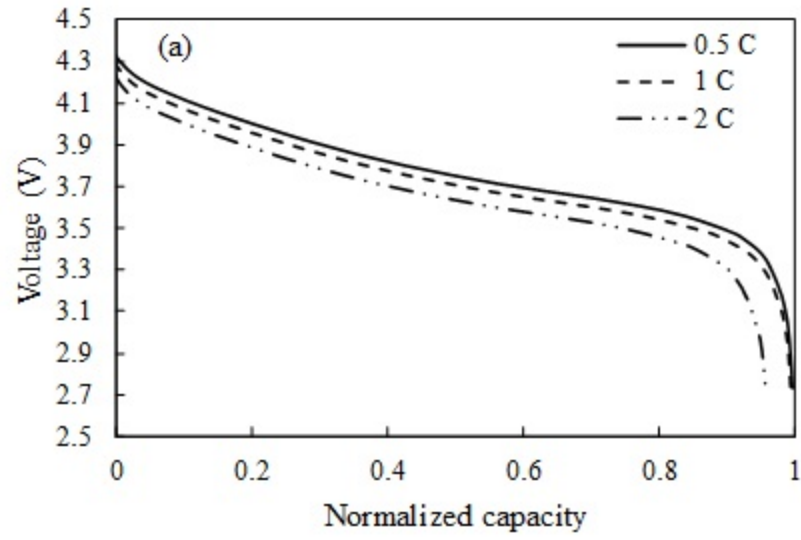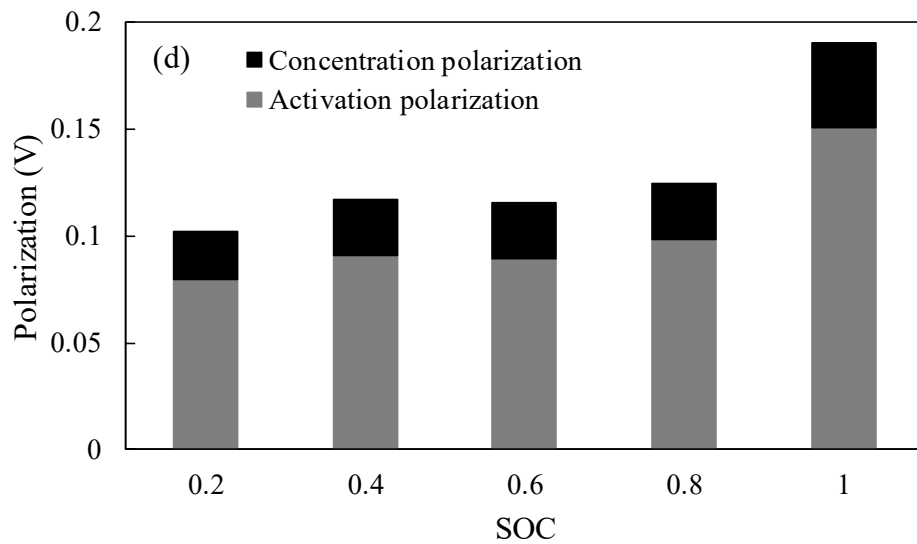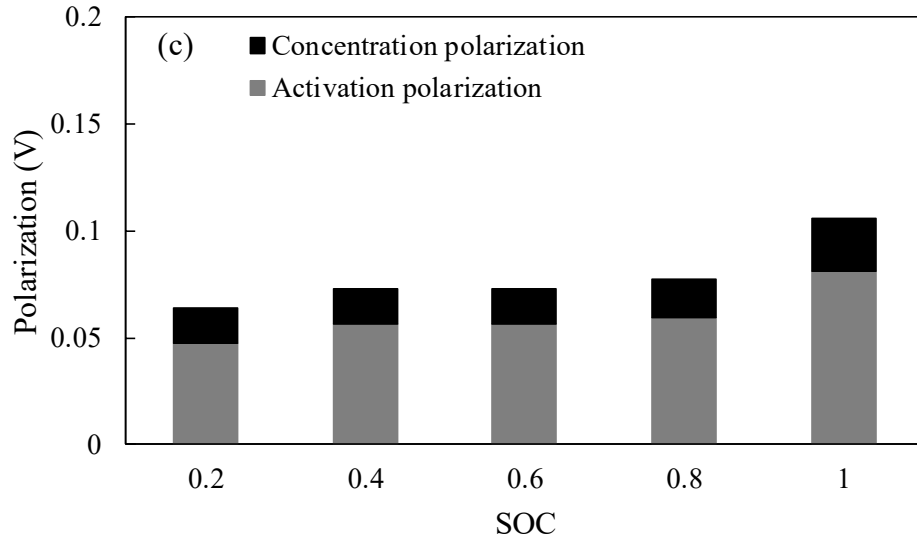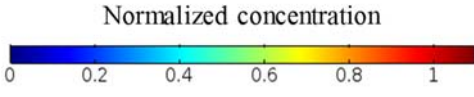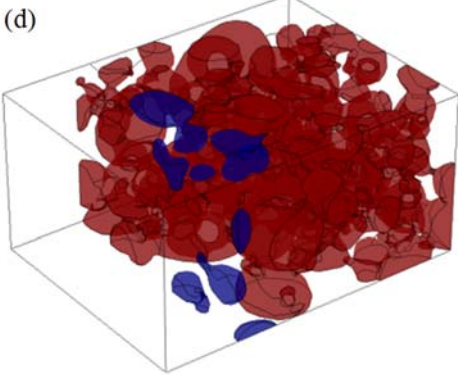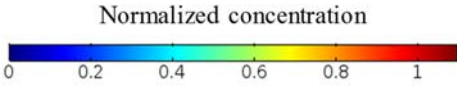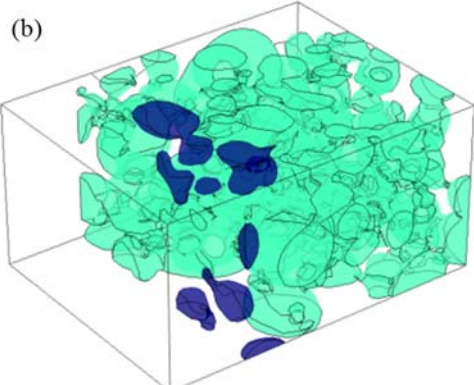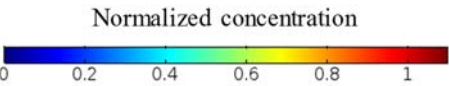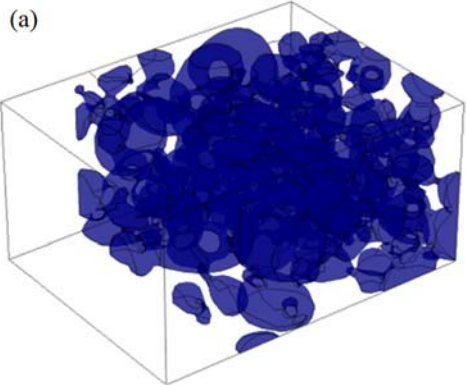
12

Fig. 2: (a) Simulated discharge curves of NMC half cell under 0.5 C, 1C and 2 C rates. Average polarization in NMC half cell (b) at 0.5 C rate, (c) at 1 C rate, and (d) at 2 C rate.

The lithium ion concentration profiles under 1 C rate are shown in Fig. 3 (a), (b), (c) and (d). Here are some features observed from Fig. 3: (i) Several particles have no lithium ion intercalation during the discharge process (see Fig. 3 (b), (c) and (d)). These particles are isolated
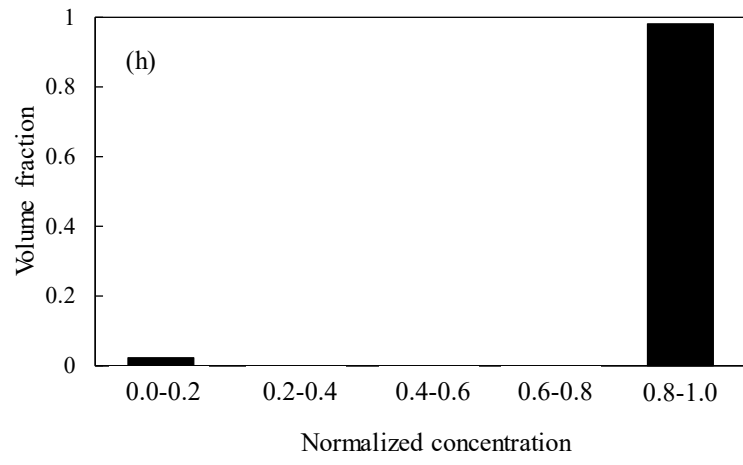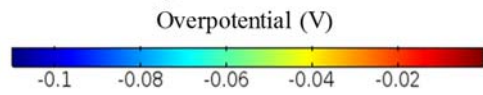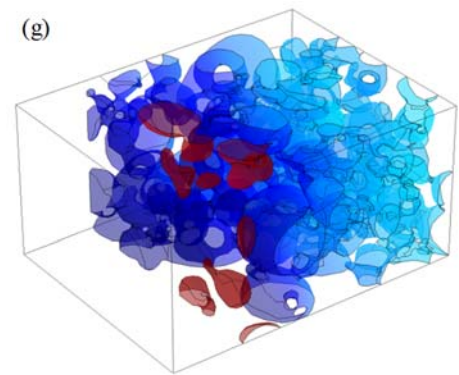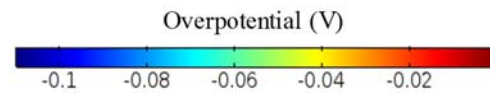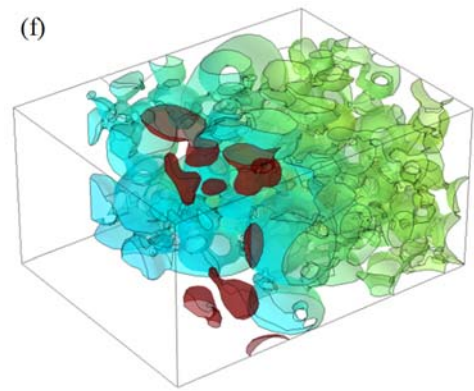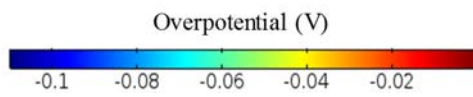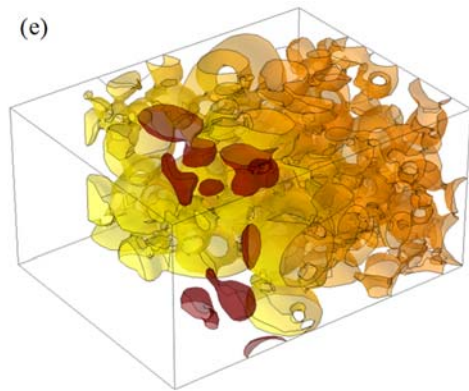
from the electrically conductive network and are not involved in electrochemical reactions. It is noted that NMC particles are only electron conductors in this model, since there is no carbon and binder phase in the model. This can also be confirmed by overpotential distributions inside the NMC half cell (see Fig. 3 (e), (f) and (g)). Several NMC particles located outside of the conductive network have zero overpotential, indicating no reactions happen in these particles. This is what traditional 1D models fail to predict; (ii) For particles in the electrochemical network, the lithium ion concentration increases during the discharge process. And the variation of the lithium ion concentration is less than 10% (see Fig. 3 (a), (b) and (d)); (iii) The lithium ion concentration is highest near the separator regions, and decreases along the thickness of the cathode (see Fig. 3 (c)). This can be evidenced by the overpotential distributions along the cathode. In overall, the overpotential has the trend to decrease along the thickness of the NMC cathode. Higher overpotential leads to higher reaction current density and lithium flux. In addition, the small particles near the separator have higher lithium ion concentration (case A) than the large particles (case B). The surface area plays an important role in the lithium concentration profile, because larger surface area contributes to higher lithium flux. It can be concluded that the small particles near the separator have the highest lithium ion concentration in the cathode, while the large particles away from the separator have the smallest.

The effect of discharge rate on local lithium distribution is shown in Fig. 3 (h), (i) and (j). It is noted that the group in 0-0.2 concentration represents the volume fraction of the isolated particles. At 0.5 C discharge rate, there is no obvious effect on local lithium accumulation. At moderate discharge rate, e.g., 1 C, the inhomogeneous NMC microstructure divides the concentration distribution into multiple groups. About 15% amount of active material is unutilized. At high discharge rate, e.g., 2 C, the microstructure inhomogeneity causes a huge impact on local

lithium accumulation. The local lithium concentration is broadening. The inhomogeneous lithium distribution in NMC cathode leads to 30% of active materials not utilized.
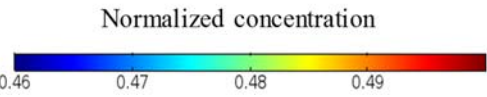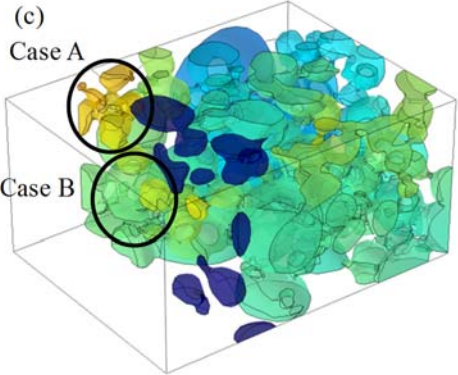
(e)

Overpotential (V)

-0.1   -0.08   -0.06   -0.04   -0.02

(f)

Overpotential (V)

-0.1   -0.08   -0.06   -0.04   -0.02

(g)

Overpotential (V)

-0.1   -0.08   -0.06   -0.04   -0.02

(h)

Normalized concentration

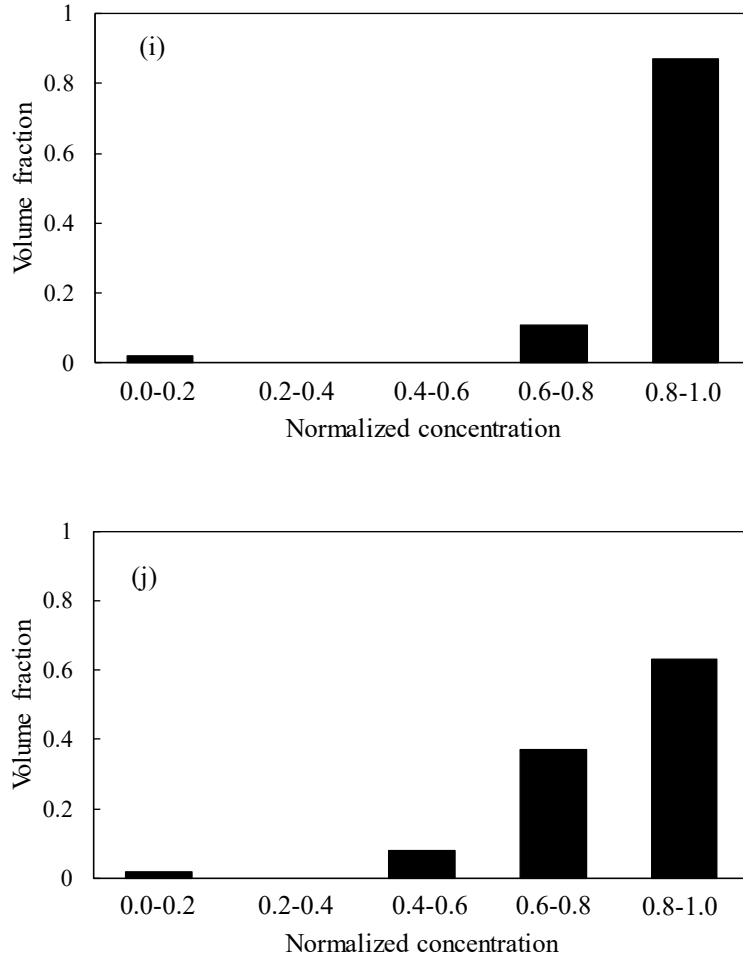Fig. 3: Lithium ion concentration in NMC particles under 1 C rate. (a) SOC=0. (b) and (c) both

shows the lithium ion concentration ar SOC=0.5, but with the color bar scale compressed in (c).

(d) SOC=1.1. Overpotential distribution in NMC half cell at the end of (e) 0.5 C rate, (f) 1 C rate,

and (g) 2 C rate. Lithium ion concentration population at the end of (h) 0.5 C rate, (i) 1 C rate, and
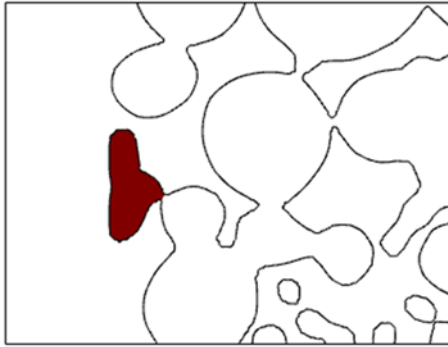
(j) 2 C rate.

4.2 Stress response

The maximum von Mises stresses in NMC particles under 0.5 C, 1 C and 2 C rates are shown in Fig. 4 (a). The maximum von Mises stresses under different C rates increase at the initial stage as lithium ions intercalates into particles. As the discharge process goes further, the stress levels go up dramatically around SOC=1, and then drop down after. The phase transition of NMC particles lead to this phenonmenon. With the increase of the lithium ion concentration, some NMC particles experience phase transition from layered structure to spinel structure around SOC=1. The phase transition introduces an abrupt volume change and generates strain mismatch, causing the stresses increase. With further electrochemical reactions, all NMC particles inside the electrochemical network change into spinel structure, and the strain mismatch is eliminated. This is further confirmed by Fig. 4 (b) and (c). At SOC=1, only the NMC particles near the separator turn into spinel structure, while all the particles in the conductive channel become spinel structure at the end of discharge. With the increase of the discharging current density, the maximum von Mises stresses increase. The maximum von Mises stresses occur after phase transition. The maximum stress at 2 C is 217.52 MPa, which is about 2 times larger than the 1 C case and 4 times larger than the 0.5 C case. The stresses tend to reach the maximum at higher SOC with the increaseing C rates. For example, the maximum von Mises stress occurs in NMC particles at SOC=1.008 under 0.5 C rate, while the stress reaches the maximum at SOC=1.01 for 1 C rate and at 1.025 for 2 C rate. It is noted that the stresses calculated in this work are one magnitude higher than the stresses in other studies. The maximum von Mises stress of $Li_xMn_2O_4$ in Zhang's work [15] is about 48 MPa. And in Lim's study [8], the maximum stress in Li_xCoO_2 particle is about 20 MPa. Considering phase transition inside the battery materials can have large influence on stress levels. Once the maximum von Mises stress inside the particles reaches the yield strength, the

mechanical failure will occur in NMC cathode. The yield strength of NMC is not available in the literature and hence we chose LiCoO₂ as the reference, since it has a similar lattice structure and composition. The yield strength of $LiCoO_2$ measured by Malav *et al.* [31] is about 200 MPa, which is lower than the maximum stress 217.52 MPa in this study. This implies the mechanical degradation will occur in NMC cathode discharging beyond 2 C rate.
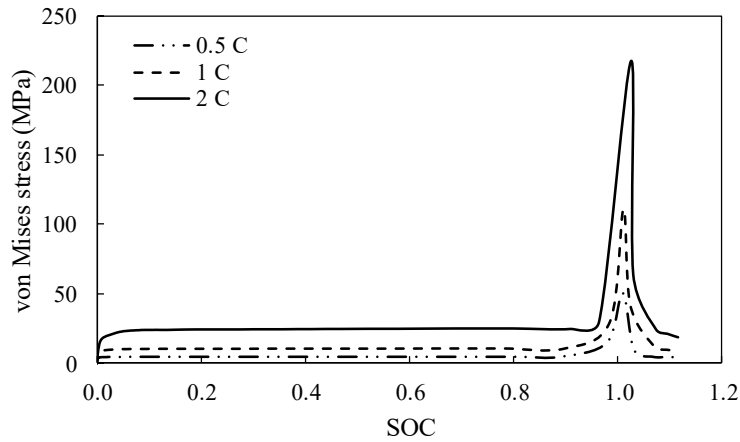
(a)
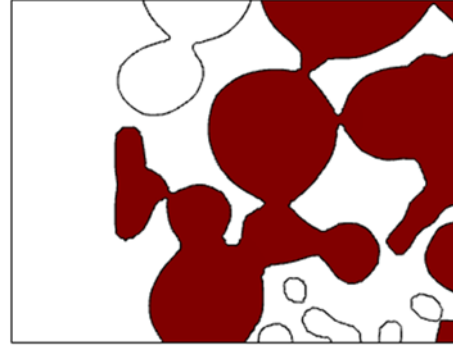
(b)   (c)

Fig. 4: (a)Time history of maximum von Mises stresses in NMC particles under 0.5 C, 1 C and 2 C rates. (b) spinel NMC at SOC=1 under 1 C rate. (c) spinel NMC at SOC=1.1 under 1 C rate. Red represents spinel NMC. The figures (b) and (c) are taken from the cross section of the half cell positioned at x=16.5 μm in Fig. 1.

It is noted that there is sharp drop in stresses after SOC=1. To take into accounts for this phenomenon, different components of strain where the maximum von Mises stresses occur were calculated. The total strain consists of intercalation strain, phase transition strain and mechanical strain, as illustrated in equation (9). As shown in Fig. 5 (a), the intercalation strain increases monotonically with the increasing SOC, where phase transition strain experiences a sudden increase near SOC=1. For the mechanical strain (see Fig. 5 (b)), the off diagonal strain components exibit small values compared with the diagonal strain. The diagonal strain components show compression features and experince sudden increase in magnitute near SOC=1. During the discharge, the intercalation and phase transition expand NMC particles while the negative elastic deformation restores the volume. The total strain was obtained by summing up intercalation, phase transition and mechanical strain, as shown in Fig. 5 (c). With the competitions of these three components, the total strain has a sudden drop after SOC=1, which has a similar feature as the maximum von Mises stresses.
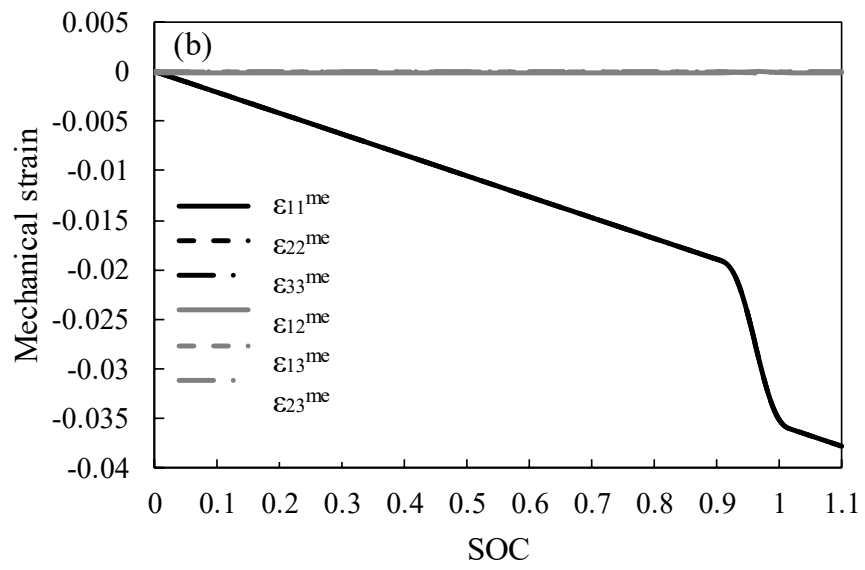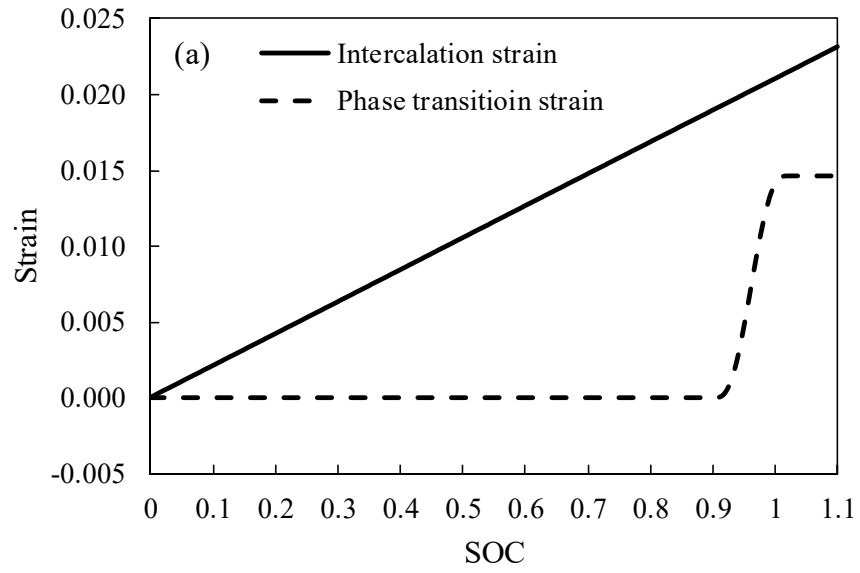
(a)

Intercalation strain
Phase transitioin strain

(b)

ε_{11}^{me}
ε_{22}^{me}
ε_{33}^{me}
ε_{12}^{me}
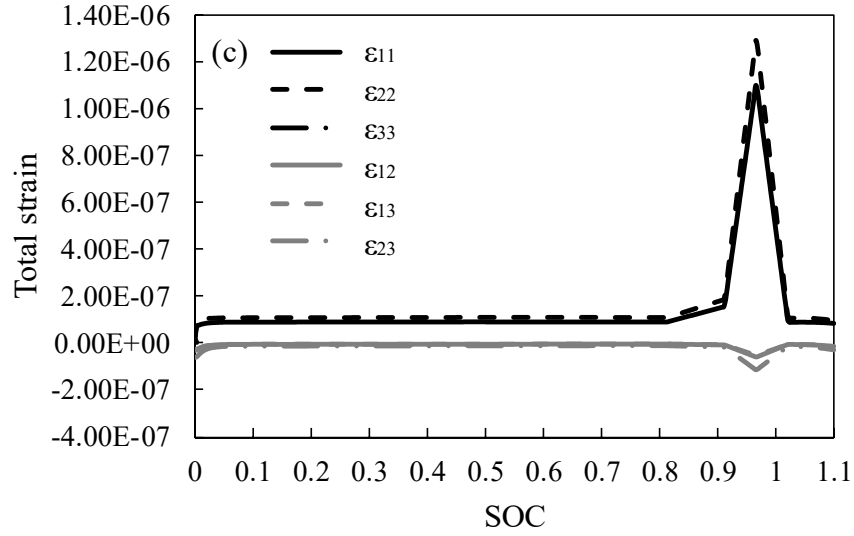ε_{13}^{me}
ε_{23}^{me}

Fig. 5: Strain where maximum von Mises stress occurs during 1 C-rate discharge. (a) intercalation and phase transition strain; (b) mechanical strain; (c) total strain.

The maximum hydrostatic stress and maximum shear stresses in NMC particles under different discharge C rates are shown in Fig. 6. In all of the three cases, hydrostatic stress is dominant and much higher than the shear stresses. The hydrostatic stress keeps increasing with the increasing SOC, and has abrupt increase near SOC=1. This is due to the lattice volume expansion introduced by phase transition. Furthermore, the hydrostatic stress increases with the rates of discharge. Hence, with the increasing discharge rates, the hydrostatic stress causes the von Mises stresses go up and fracture are more likely to occur due to the hydrostatic stress.
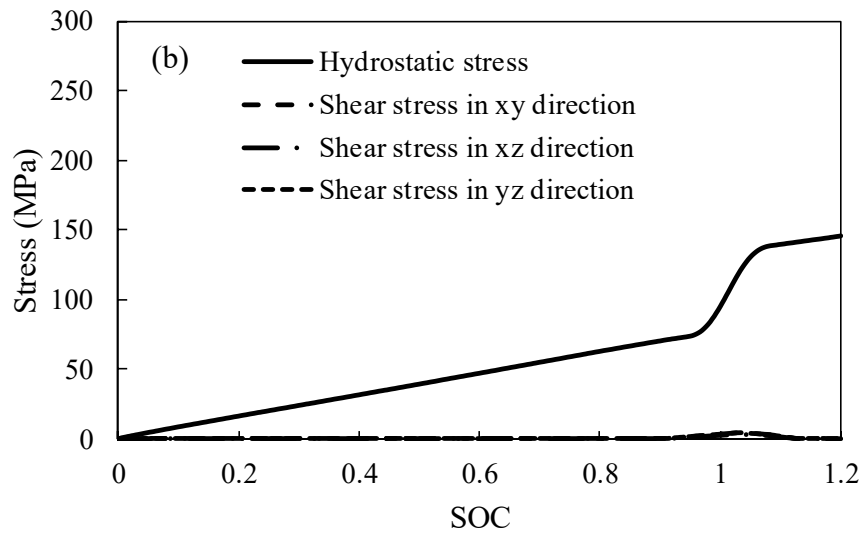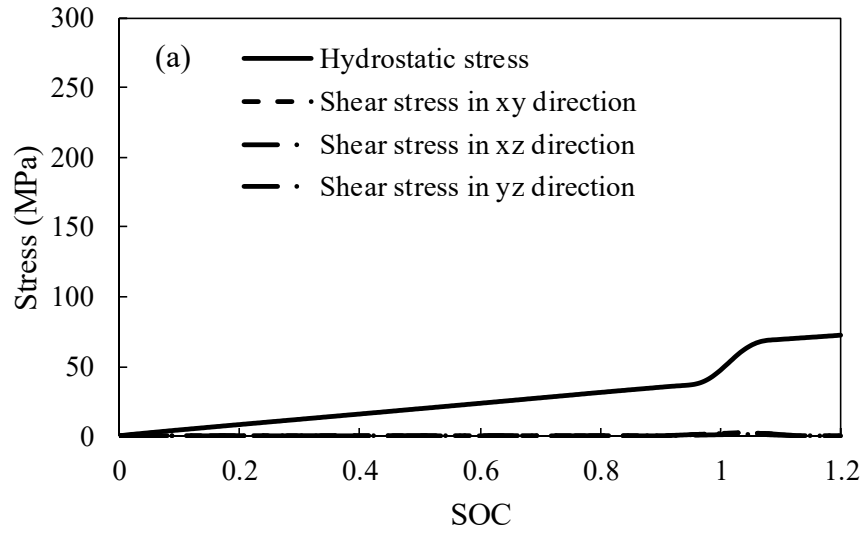
Fig. 6: Maximum hydrostatic stress and maximum shear stresses in NMC particles under different C-rates. (a) 0.5 C; (b) 1 C; (c) 2 C.
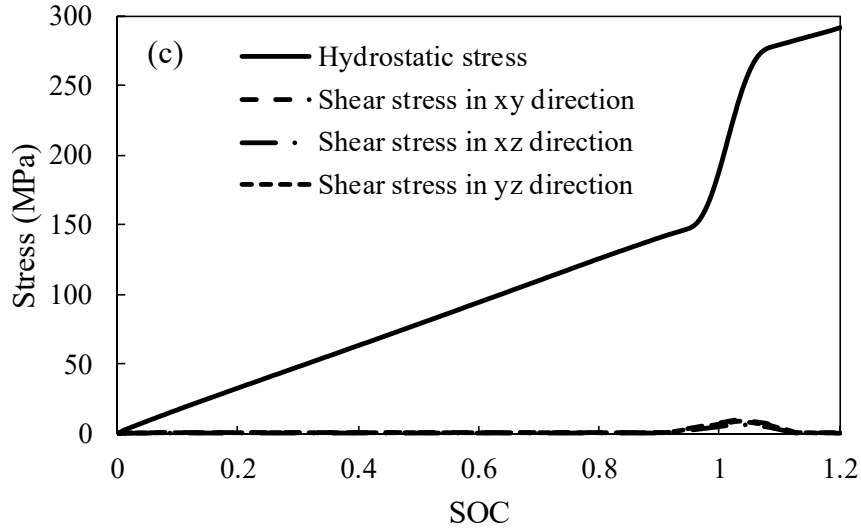
To better understand the failure mechanisms in the NMC half cell, the stress distribution inside the particles was investigated. In Fig. 7, the von Mises stresses inside the NMC particles at SOC=1 under 1 C rate is shown. Unlike the uniform stress distribution in the 1D model [32] and single particle model [15], the von Mises stress distribution shows a strong geometry effect. Here are some observations for stress distribution: (1) For the particles isolated from the electrochemical network, the stresses are zero (case A). Since there is no lithium ion intercalation inside these particles, stress will not be generated by diffusion and phase transitions. (2) The concave and convex regions are the most critical places where the mechanical failure may occur. The von Mises stresses near these regions are much higher than other areas (case B). (3) Away from the stress concentration regions, the stresses on the surfaces of NMC particles are higher than the stresses inside the particles (case C). Since the stresses near the concave and covex regions are the highest,

the cracks may be initiated in these regions. Once the cracks propogate, the neck regions of the connected particles will break and form several isolated particles. If the isolated particles are not connected with the electrically conductive materials such as carbon and binder, the capacity will lose in LIBs. For isolated particles in the conductive channel, cracks are more likely to form on the surface. Eventually, the particles will break into several small particles.
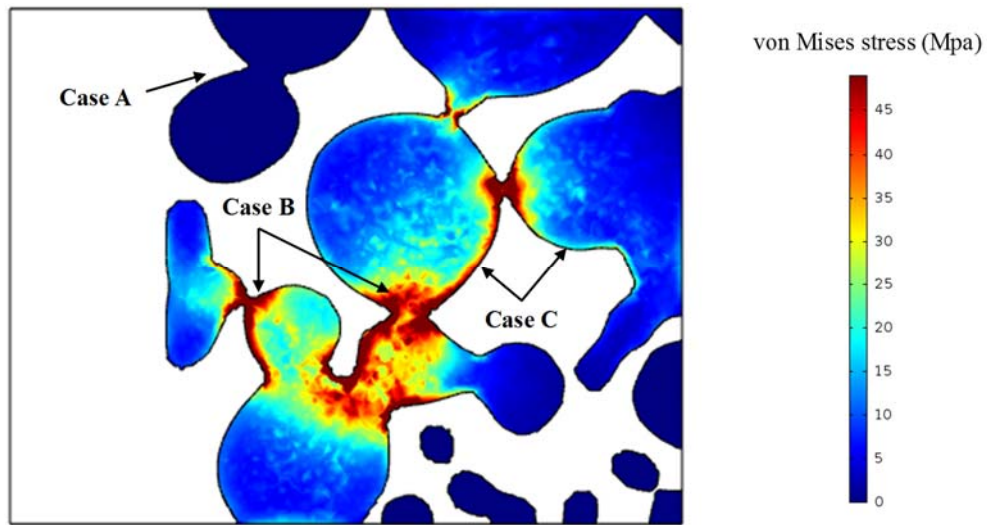

Fig. 7: von Mises stresses distribution in reconstructed NMC particles at SOC=1 under 1 C rate. The figure is taken from the cross section of the half cell which positioned at x=16.5 μm in Fig. 1.

To study the geometry effect more quantitatively, the stress distribution near the convex and concave regions was investigated. In the study, four points were selected to represent the concave and convex regions, as shown in Fig. 8 (a). A and C represent the concave regions, while B and D represent the convex regions. The von Mises stresses time history of four points under 1 C rate is shown in Fig. 8 (b). The von Mises stresses of all of the four points show similar patterns as Fig. 4 (a). The stresses increase at the initial stage. As the discharge process goes further, the maximum von Mises stresses increase dramatically because of the phase transition, and then drop

down. The stresses of two concave points A and C are significantly higher than thier corresponding convex points B and D. The maximum von Mises stress of point A is 67.5 MPa, which is 49% higher than the stress of point B. The stress of point C is 22.5 MPa, which is four times the stress in its correspoonding convex point D. Hence, the stresses in the concave points are more critical than the convex points.
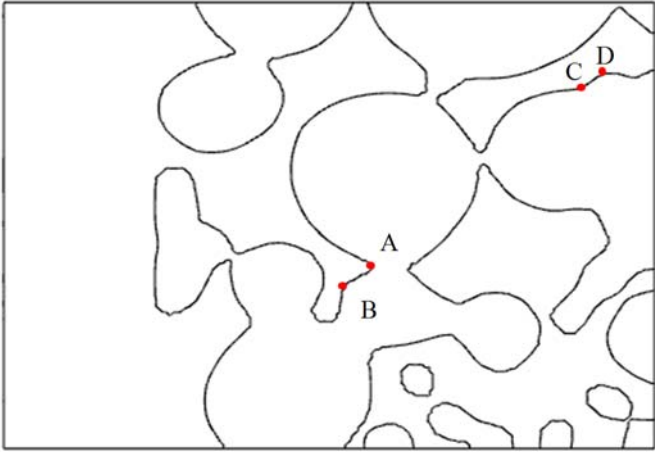
(a)
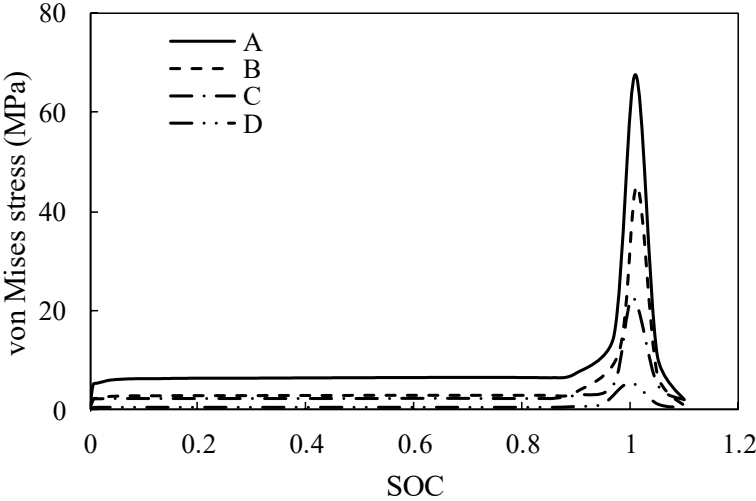
(b)

Fig. 8: (a): The positions of four selected points A, B, C and D. (b) The von Mises stresses time history of four selected points A, B, C and D under 1 C rate.

5. Conclusions

The electrochemical properties and stress generation caused by phase transition and intercalation in NMC, with realistic 3D microstructures from synchrotron X-ray tomography, have been investigated using finite element method. The conclusions are summarized as follows:

(1) The discharged curves under various C rates are simulated. The potential drops significantly with the increase of C rates due to the increasing internal resistance.

(2) During the discharge process, for particles isolated from the conductive channel, several particles without lithium ion intercalation are observed. For particles in the electrochemical network, the lithium ion concentration increases during the discharge process. The variation of the lithium ion concentration is less than 10%.

(3) Stresses inside the particles increase dramatically when considering phase transitions. The phase transition introduce an abrupt volume change and generate the strain mismatch, causing the stresses increase. With the increase of the discharging current density, the maximum von Mises stresses increase.

(4) For the particles away from the electrochemical network, they remain unstressed during the discharge process. The concave and convex regions are the most critical places where the mechanical failure may occur. Away from the stress concentration regions, the stresses on the surface of the NMC particles are higher than the stresses inside the particles.

(5) The maximum von Mises stress is more likely to occur at concave regions rather than convex regions. The study shows the von Mises stresses in the concave region can be four times larger than the convex region.

Acknowledgment

List of Figures

Fig. 1: (a) Raw synchrotron X-ray reconstructed NMC cathode's cross sectional view before image processing. White color represents NMC particles and black colar represents electrolyte. (b) Cross sectional view of NMC cathode after image processing. White color represents NMC particles and black colar represents electrolyte. (c) Three-dimensional finte element mesh of the NMC half cell. Red color represents NMC particles and blue color represents electrolyte.

Fig. 2: (a) Simulated discharge curves of NMC half cell under 0.5 C, 1C and 2 C rates. Average polarization in NMC half cell (b) at 0.5 C rate, (c) at 1 C rate, and (d) at 2 C rate.

Fig. 3: Lithium ion concentration in NMC particles under 1 C rate. (a) SOC=0. (b) and (c) both shows the lithium ion concentration ar SOC=0.5, but with the color bar scale compressed in (c). (d) SOC=1.1. Overpotential distribution in NMC half cell at the end of (e) 0.5 C rate, (f) 1 C rate, and (g) 2 C rate. Lithium ion concentration population at the end of (h) 0.5 C rate, (i) 1 C rate, and (j) 2 C rate.

Fig. 4: (a)Time history of maximum von Mises stresses in NMC particles under 0.5 C, 1 C and 2 C rates. (b) spinel NMC at SOC=1 under 1 C rate. (c) spinel NMC at SOC=1.1 under 1 C rate. Red represents spinel NMC. The figures (b) and (c) are taken from the cross section of the half cell positioned at x=16.5 μm in Fig. 1.

Fig. 5: Strain where maximum von Mises stress occurs during 1 C-rate discharge. (a) intercalation and phase transition strain; (b) mechanical strain; (c) total strain.

Fig. 6: Maximum hydrostatic stress and maximum shear stresses in NMC particles under different C-rates. (a) 0.5 C; (b) 1 C; (c) 2 C.

Fig. 7: von Mises stresses distribution in reconstructed NMC particles at SOC=1 under 1 C rate. The figure is taken from the cross section of the half cell which positioned at x=16.5 μm in Fig. 1.

Fig. 8: (a): The positions of four selected points A, B, C and D. (b) The von Mises stresses time history of four selected points A, B, C and D under 1 C rate.

List of Tables

References

[1]   J. M. Tarascon and M. Armand, "Issues and challenges facing rechargeable lithium batteries," *Nature,* vol. 414, pp. 359-367, 11/15/print 2001.

[2]   D. R. Ely and R. E. García, "Heterogeneous Nucleation and Growth of Lithium Electrodeposits on Negative Electrodes," *Journal of The Electrochemical Society,* vol. 160, pp. A662-A668, 2013.

[3]   K. J. Harry, D. T. Hallinan, D. Y. Parkinson, A. A. MacDowell, and N. P. Balsara, "Detection of subsurface structures underneath dendrites formed on cycled lithium metal electrodes," *Nat Mater,* vol. 13, pp. 69-73, 2014.

[4]   J. Xu, R. D. Deshpande, J. Pan, Y.-T. Cheng, and V. S. Battaglia, "Electrode Side Reactions, Capacity Loss and Mechanical Degradation in Lithium-Ion Batteries," *Journal of The Electrochemical Society,* vol. 162, pp. A2026-A2035, 2015.

[5]   C. K. Chan, R. Ruffo, S. S. Hong, R. A. Huggins, and Y. Cui, "Structural and electrochemical study of the reaction of lithium with silicon nanowires," *Journal of Power Sources,* vol. 189, pp. 34-39, 2009.

[6]   D. P. Finegan, M. Scheel, J. B. Robinson, B. Tjaden, I. Hunt, T. J. Mason*, et al.*, "In-Operando High-Speed Tomography of Lithium-Ion Batteries During Thermal Runaway," *Nature Communnications,* vol. 6, 2015.

[7]   C. F. Lopez, J. A. Jeevarajan, and P. P. Mukherjee, "Experimental Analysis of Thermal Runaway and Propagation in Lithium-Ion Battery Modules," *Journal of The Electrochemical Society,* vol. 162, pp. A1905-A1915, 2015.

[8]   C. Lim, B. Yan, L. Yin, and L. Zhu, "Simulation of Diffusion-Induced Stress Using Reconstructed Electrodes Particle Structures Generated by Micro/Nano-CT," *Electrochimica Acta,* vol. 75, pp. 279-287, 2012.

[9]   L. Wu, Y. Zhang, Y.-G. Jung, and J. Zhang, "Three-Dimensional Phase Field Based Finite Element Study on Li Intercalation-Induced Stress in Polycrystalline $LiCoO_2$," *Journal of Power Sources,* vol. 299, pp. 57-65, 2015.

[10]   J. Park, W. Lu, and A. M. Sastry, "Numerical Simulation of Stress Evolution in Lithium Manganese Dioxide Particles due to Coupled Phase Transition and Intercalation," *Journal of The Electrochemical Society,* vol. 158, pp. A201-A206, 2011.

[11]   S. Renganathan, G. Sikha, S. Santhanagopalan, and R. E. White, "Theoretical Analysis of Stresses in a Lithium Ion Cell," *Journal of The Electrochemical Society,* vol. 157, pp. A155-A163, 2010.

[12]   K. Zhao, M. Pharr, J. J. Vlassak, and Z. Suo, "Fracture of electrodes in lithium-ion batteries caused by fast charging," *Journal of Applied Physics,* vol. 108, p. 073517, 2010.

[13]   Y.-T. Cheng and M. W. Verbrugge, "Evolution of stress within a spherical insertion electrode particle under potentiostatic and galvanostatic operation," *Journal of Power Sources,* vol. 190, pp. 453-460, 2009.

[14]   X. Zhang, A. M. Sastry, and W. Shyy, "Intercalation-Induced Stress and Heat Generation within Single Lithium-Ion Battery Cathode Particles," *Journal of The Electrochemical Society,* vol. 155, pp. A542-A552, 2008.

[15]   X. Zhang, W. Shyy, and A. Marie Sastry, "Numerical Simulation of Intercalation-Induced Stress in Li-Ion Battery Electrode Particles," *Journal of The Electrochemical Society,* vol. 154, pp. A910-A916, 2007.

[16]   L. Wu and J. Zhang, "Ab initio study of anisotropic mechanical properties of LiCoO2 during lithium intercalation and deintercalation process," *Journal of Applied Physics,* vol. 118, p. 225101, 2015.

[17]   W. Wu, X. Xiao, M. Wang, and X. Huang, "A Microstructural Resolved Model for the Stress Analysis of Lithium-Ion Batteries," *Journal of The Electrochemical Society,* vol. 161, pp. A803-A813, 2014.

[18]   M. Doyle, T. F. Fuller, and J. Newman, "Modeling of Galvanostatic Charge and Discharge of the Lithium/Polymer/Insertion Cell," *Journal of The Electrochemical Society,* vol. 140, pp. 1526-1533, 1993.

[19]   T. F. Fuller, M. Doyle, and J. Newman, "Simulation and Optimization of the Dual Lithium Ion Insertion Cell," *Journal of The Electrochemical Society,* vol. 141, pp. 1-10, 1994.

[20]   F. Yang, "Interaction between diffusion and chemical stresses," *Materials Science and Engineering: A,* vol. 409, pp. 153-159, 2005.

[21]   J. Newman, "Electrochemical Systems, 3rd Ed.," *Wiley Inter-science, United States,* 2004.

[22]   M. Gu, I. Belharouak, J. Zheng, H. Wu, J. Xiao, A. Genc*, et al.*, "Formation of the Spinel Phase in the Layered Composite Cathode Used in Li-Ion Batteries," *ACS Nano,* vol. 7, pp. 760-767, 2013.

[23]   I. Buchberger, S. Seidlmayer, A. Pokharel, M. Piana, J. Hattendorff, P. Kudejova*, et al.*, "Aging Analysis of Graphite/LiNi$_{1/3}$Mn$_{1/3}$Co$_{1/3}$O$_2$ Cells Using XRD, PGAA, and AC Impedance," *Journal of The Electrochemical Society,* vol. 162, pp. A2737-A2746, 2015.

[24]   W. Wu, X. Xiao, and X. Huang, "The effect of battery design parameters on heat generation and utilization in a Li-ion cell," *Electrochimica Acta,* vol. 83, pp. 227-240, 2012.

[25]   C. R. Birkl, E. McTurk, M. R. Roberts, P. G. Bruce, and D. A. Howey, "A Parametric Open Circuit Voltage Model for Lithium Ion Batteries," *Journal of The Electrochemical Society,* vol. 162, pp. A2271-A2280, 2015.

[26]   Q. Zhang and R. E. White, "Capacity fade analysis of a lithium ion cell," *Journal of Power Sources,* vol. 179, pp. 793-798, 5/1/ 2008.

[27]   R. Amin and Y.-M. Chiang, "Characterization of Electronic and Ionic Transport in Li$_{1-x}$Ni$_{0.33}$Mn$_{0.33}$Co$_{0.33}$O$_2$ (NMC333) and Li$_{1-x}$Ni$_{0.50}$Mn$_{0.20}$Co$_{0.30}$O$_2$ (NMC523) as a Function of Li Content," *Journal of The Electrochemical Society,* vol. 163, pp. A1512-A1517, 2016.

[28]   L. S. d. Vasconcelos, R. Xu, J. Li, and K. Zhao, "Grid Indentation Analysis of Mechanical Properties of Composite Electrodes in Li-Ion Batteries," *Extreme Mechanics Letters,* vol. In Press, 2016.

[29]   O. Dolotko, A. Senyshyn, M. J. Mühlbauer, K. Nikolowski, and H. Ehrenberg, "Understanding Structural Changes in NMC Li-Ion Cells by *In Situ* Neutron Diffraction," *Journal of Power Sources,* vol. 255, pp. 197-203, 2014.

[30]   A. Nyman, T. G. Zavalis, R. Elger, M. Behm, and G. Lindbergh, "Analysis of the Polarization in a Li-Ion Battery Cell by Numerical Simulations," *Journal of The Electrochemical Society,* vol. 157, pp. A1236-A1246, 2010.

[31]   V. Malav, M. K. Jangid, I. Hait, and A. Mukhopadhyay, "In Situ Monitoring of Stress Developments and Mechanical Integrity during Galvanostatic Cycling of LiCoO2 Thin Films," *ECS Electrochemistry Letters,* vol. 4, pp. A148-A150, 2015.

[32]   W. Wu, X. Xiao, X. Huang, and S. Yan, "A multiphysics model for the in situ stress analysis of the separator in a lithium-ion battery cell," *Computational Materials Science,* vol. 83, pp. 127-136, 2014.